1-9-2017

Dominance of grain size impacts on seasonal snow albedo at deforested sites in New Hampshire

Alden C. Adolph
Dartmouth College

Mary R. Albert
Dartmouth College

James Lazarcik
University of New Hampshire, Durham

Jack E. Dibb
University of New Hampshire, Durham, jack.dibb@unh.edu

Jacqueline M. Amante
University of New Hampshire, Durham

See next page for additional authors

Follow this and additional works at: https://scholars.unh.edu/ersc

Authors

Alden C. Adolph, Mary R. Albert, James Lazarcik, Jack E. Dibb, Jacqueline M. Amante, and Andrea Price

JGR

RESEARCH ARTICLE

Key Points:
- The most important driver for snow albedo changes in New Hampshire is grain size evolution
- Winter storm trajectories in the northeastern U.S. impact resulting snow properties
- 52% of variability in broadband albedo in New Hampshire snow can be parameterized by using mean temperature and days since snowfall

Supporting Information:
- Supporting Information S1

Correspondence to:
A. C. Adolph,
Alden.C.Adolph.TH@Dartmouth.edu

Dominance of grain size impacts on seasonal snow albedo at open sites in New Hampshire

Alden C. Adolph[1] (ID), **Mary R. Albert[1]** (ID), **James Lazarcik[2,3]** (ID), **Jack E. Dibb[2,3]** (ID), **Jacqueline M. Amante[2,3]**, and **Andrea Price[1]**

[1]Thayer School of Engineering, Dartmouth College, Hanover, New Hampshire, USA, [2]Department of Earth Science, University of New Hampshire, Durham, New Hampshire, USA, [3]Institute for the Study of Earth, Oceans, and Space, University of New Hampshire, Durham, New Hampshire, USA

Abstract Snow cover serves as a major control on the surface energy budget in temperate regions due to its high reflectivity compared to underlying surfaces. Winter in the northeastern United States has changed over the last several decades, resulting in shallower snowpacks, fewer days of snow cover, and increasing precipitation falling as rain in the winter. As these climatic changes occur, it is imperative that we understand current controls on the evolution of seasonal snow albedo in the region. Over three winter seasons between 2013 and 2015, snow characterization measurements were made at three open sites across New Hampshire. These near-daily measurements include spectral albedo, snow optical grain size determined through contact spectroscopy, snow depth, snow density, black carbon content, local meteorological parameters, and analysis of storm trajectories using the Hybrid Single-Particle Lagrangian Integrated Trajectory model. Using analysis of variance, we determine that land-based winter storms result in marginally higher albedo than coastal storms or storms from the Atlantic Ocean. Through multiple regression analysis, we determine that snow grain size is significantly more important in albedo reduction than black carbon content or snow density. And finally, we present a parameterization of albedo based on days since snowfall and temperature that accounts for 52% of variance in albedo over all three sites and years. Our improved understanding of current controls on snow albedo in the region will allow for better assessment of potential response of seasonal snow albedo and snow cover to changing climate.

1. Introduction

Seasonal and perennial snow cover serve as important climate regulators on regional and global scales due to the high albedo of snow. Any amount of snowmelt that exposes the underlying ground surface typically causes a reduction in the overall albedo and a corresponding temperature increase in a process known as the snow albedo feedback [e.g., *Groisman et al.*, 1994]. Northern Hemisphere snow cover extent in spring has been decreasing by 11.7% per decade since 1967 [*Intergovernmental Panel on Climate Change*, 2013] due to higher temperatures that are amplified by the snow albedo feedback [*Déry and Brown*, 2007; *Brown and Mote*, 2009]. Additionally, the seasonal snow cover and albedo are sensitive to precipitation rates and the partitioning between snow and rain events during the winter season. While precipitation is projected to increase globally, and specifically in the New England area, a larger fraction of the precipitation is expected to fall as rain [*Huntington et al.*, 2004; *Knowles et al.*, 2006; *Trenberth*, 2011], and changes in midlatitude storm patterns are expected [*Cohen et al.*, 2014].

Changes in snow albedo, and in turn snowmelt, are important to local communities, as snowmelt is often a source for water reservoirs and can also result in flooding during rapid melt events [e.g., *Barnett et al.*, 2005; *Qian et al.*, 2009; *Painter et al.*, 2010]. Timing of snowmelt is also linked to plant and animal phenology, where changes in seasonal transitions can impact a series of ecosystem functions [e.g., *White et al.*, 2009; *Peng et al.*, 2013; *Contosta et al.*, 2016]. In New Hampshire, persistent deep snow cover is especially important because winter recreation and tourism are critical components of the state economy [*Burakowski and Magnusson*, 2012; *Hamilton et al.*, 2003]. Despite these important implications of changes in snow cover and snow properties, there is very little published information about snow albedo in New England.

Snow albedo is a critical component of climate models because of the temperature feedback associated with melting snow [*Hall and Qu*, 2006; *Déry and Brown*, 2007; *Qu and Hall*, 2007]. As melting snow reveals the underlying ground, which has a lower albedo, more of the incoming solar radiation is absorbed, thus

increasing the surface temperature. Though this feedback is important, it is not well quantified. There is a consistent spread in the strength of the snow albedo feedback across models as indicated by the results of the Coupled Model Intercomparison Project Phase 5 [*Qu and Hall*, 2014]. Model differences are largely due to the way that albedo is parameterized, where models with higher albedo result in a higher sensitivity to the snow albedo feedback. Variability exists in the albedo values used for both open and forested snow-covered areas, and it is the variability among the fully snow-covered areas that results in the most significant difference [*Fletcher et al.*, 2012; *Qu and Hall*, 2007]. Despite the fact that snow albedo can have such a dramatic effect, parameterizations to account for variability in albedo are not yet well constrained and could benefit from increased observations of surface albedo [*Qu and Hall*, 2007].

Many efforts have been made to incorporate variability in snow albedo models. Examples include work done by *Flanner et al.* [2007] and *Slater et al.* [1998] that contain dependencies on grain size and impurity content, known to influence overall albedo [e.g., *Wiscombe and Warren*, 1980; *Warren and Wiscombe*, 1980]. *Flanner et al.* [2007] developed the Snow, Ice, and Aerosol Radiation Model (SNICAR), which was then used to assess the climate forcing of black carbon. They concluded that black carbon emissions are the largest source of uncertainty in the estimated forcing, and snow aging was the second largest source of uncertainty. As snow ages the grain size increases, which reduces albedo directly but also enhances the albedo reduction caused by black carbon presence. Consequently, snow albedo is particularly hard to capture at the end of the season, when parameterizing albedo is most important [*Slater et al.*, 1998]. Better understanding of the process of albedo reduction in aging and melting snow is required.

Snow albedo is controlled by the optical properties of the constituent parts of snow: ice, air, and impurities in the snowpack. Impurity loading and the grain size of the snow are two of the most critical factors determining snow albedo because changes in each can have an effect on their own, and the interactions between impurities and snow microphysics are hypothesized to reinforce each other, although the magnitude and rates of these feedback between impurities and snow grain characteristics are poorly quantified [*Flanner et al.*, 2007]. *Wiscombe and Warren* [1980] outline external factors that impact the albedo, such as solar zenith angle and direct versus diffuse lighting conditions, as well as intrinsic physical and chemical properties of the snowpack that affect the way that light interacts with the snow. When a snowpack is shallow, the albedo of the underlying medium will impact the overall surface albedo. The impact of the surface below reduces as the snowpack thickens, and the thickness required to consider this impact negligible depends on wavelength and snow properties. For a snowpack that is optically thick, there are well-established links between the grain size of the snow and the snow albedo, particularly in the near-infrared region of the solar spectrum where grain size has the largest effect [*Aoki et al.*, 2003; *Kokhanovsky and Zege*, 2004]. As grain size increases, scattering within the snowpack decreases and the absorbing path length within grains increases, thus reducing the overall albedo [e.g., *Wiscombe and Warren*, 1980; *Flanner and Zender*, 2006]. In the visible region, albedo is most strongly reduced by the presence of light-absorbing impurities such as dust and black carbon [e.g., *Warren and Wiscombe*, 1980], and this effect is enhanced as snow grain size increases [*Hadley and Kirchstetter*, 2012]. While impurities can have an impact on the near-infrared (NIR) albedo [*Warren and Wiscombe*, 1980; *Nolin and Dozier*, 2000; *Singh et al.*, 2010; *Skiles*, 2014], control of albedo in the NIR region is dominated by ice absorption. Variability in albedo is also linked to the snow surface roughness [*Lhermitte et al.*, 2014], density [e.g., *Flanner and Zender*, 2006; *Wiscombe and Warren*, 1980], and the liquid content of the snow during melt events [*Aoki et al.*, 2003].

To quantify the links between the physical structure of snow and resulting snow albedo, several measurement-intensive field studies have been conducted, but most of these studies have focused on polar or high-altitude regions. *Meinander et al.* [2013] used in situ data to find that the albedo of melting snow in Finland decreased compared to fresh snow due to large grains, presence of liquid water, and high contents of elemental and organic carbon. *Carmagnola et al.* [2013] used measurements in the dry snow zone of Greenland to evaluate a physically based albedo model and found that the model could determine energy absorbed within 1.1% and also that the impact of impurities on albedo is relatively small in that part of Greenland. *Pedersen et al.* [2015] found a significant correlation between black carbon content in snow and spectral albedo at four sites in the Arctic. They used these data to develop empirical formulas to determine albedo reduction based on black carbon content and grain size. Through measurements in Antarctica, *Gallet et al.* [2011] used specific surface area and density to model snow albedo for comparison with satellite-derived albedo, and *Picard et al.* [2016] developed a method to derive specific surface area of snow from spectral albedo measurements.

Table 1. Description of Measurement Sites Including the Measurement Frequency in Each Study Year

Site	Town	Location	Elevation	2013	2014	2015
CRREL Yard (CYO)	Hanover	N43°43′, W72°16′	142 m	2 times per week	6 times per week	
Dartmouth Farm (DFO)	Hanover	N43°44′, W72°15′	119 m	–	–	~daily
Thompson Farm (TFO)	Durham	N43°06′, W70°56′	19 m	2 times per week	6 times per week	~daily
Burley-Demerrit Farm (BDO)	Lee	N43°05′, W70°59′	35 m	2 times per week	6 times per week	~daily

Intensive in situ measurements of albedo and snow properties at low altitude, midlatitudes are less common, with the exception of *Perovich* [2007], who made albedo measurements in New Hampshire, U.S. in the 1990s, and *Aoki et al.* [2000, 2007, 2011], who has conducted research at a midlatitude, temperate site in Japan. Their extensive measurements of snow albedo and snow properties detailed in these three papers culminate with the development of a physically based snow albedo model, which is comparable to the SNICAR model developed by *Flanner et al.* [2007]. In the western U.S., a number of studies have been conducted on the influence of impurities on snow albedo [*Doherty et al.*, 2014, 2016; *Kaspari et al.*, 2014, 2015; *Delaney et al.*, 2015; *Painter et al.*, 2007b, 2012; *Skiles*, 2014; *Skiles et al.*, 2012, 2015]. *Skiles* [2014] collected a similar data set to ours, with daily field measurements of albedo and snow properties in the Rocky Mountains in the western U.S.. However, the literature does not contain studies of snow albedo in the eastern United States. Additionally, our data set is more comprehensive than most previous work in other regions because we measured spectral albedo and conducted analysis of the entire snowpack with depth for optical grain size, black carbon content, and snow density over 3 years. These very intensive measurements with spatial coverage of three sites and near daily temporal coverage throughout three winter seasons are the first of its kind in the eastern United States.

There is a general understanding of the physics that control the albedo of snow, but different factors dominate changes in albedo at various locations. The presence of impurities, particularly dust and black carbon, in snow is one factor that has received much attention in recent scientific research [e.g., *Ramanathan and Carmichael*, 2008; *Flanner et al.*, 2007; *Hansen and Nazarenko*, 2004; *Sterle et al.*, 2013; *Doherty et al.*, 2014, 2016; *Kaspari et al.*, 2014, 2015; *Delaney et al.*, 2015; *Painter et al.*, 2007b, 2012; *Skiles et al.*, 2015; *Polashenski et al.*, 2015; *Dang et al.*, 2015; *Oaida et al.*, 2015; *Yasunari et al.*, 2015; *Qian et al.*, 2015]. Using our extensive measurements in New Hampshire, we assess the reduction of snow albedo due to impurities in comparison to other factors. First, we determine which factors dominate the albedo of fresh snow in New Hampshire; we assess the physical and chemical properties of fresh snow and determine how these properties are related to the path of the snow storm using back trajectory analysis. Second, we analyze the evolution of snow properties and snow albedo over time throughout the winter, quantifying the sensitivities of snow albedo to optical grain size, density, and impurity content and comparing these sensitivities to the SNICAR model. Finally, we determine parameterizations of albedo based on temperature and days since snowfall, both of which are variables that are linked to metamorphism and are readily available both historically and in climate projections. This parameterization is compared to similar models that use the same input variables, and the applicability of this parameterization to other regions is discussed.

2. Methods

2.1. Field Measurements

Over the course of three winters (2013–2015), we conducted field measurements to study the albedo of New Hampshire seasonal snow. Measurements were made predominantly in January through early April, though in 2013 and 2014 at the Durham sites, measurements began in late December. Locations and details about measurement frequency are shown in Table 1, and a map indicating the location of the field sites is presented in Figure 1. The Hanover site moved from Cold Regions Research and Engineering Laboratory (CRREL) Yard to the Dartmouth Farm (DFO) in 2015 because the DFO site is more similar to the Durham sites and had a larger open area available for spatial survey work. The field measurement campaign was designed to study the seasonal snow albedo throughout the winter and also to look at dynamics within the snowpack such as the movement of ions and impurities as well as the evolution of grain shape and size. Measurements were made within an hour of solar noon to attain the lowest solar zenith angle possible during albedo measurement.

We measured snow albedo by using an Analytical Spectral Devices (ASD) FieldSpec4 Standard Resolution spectrometer. This instrument has a spectral sampling (bandwidth) of 1.1 to 1.4 nm from 350 nm to 2500 nm. The
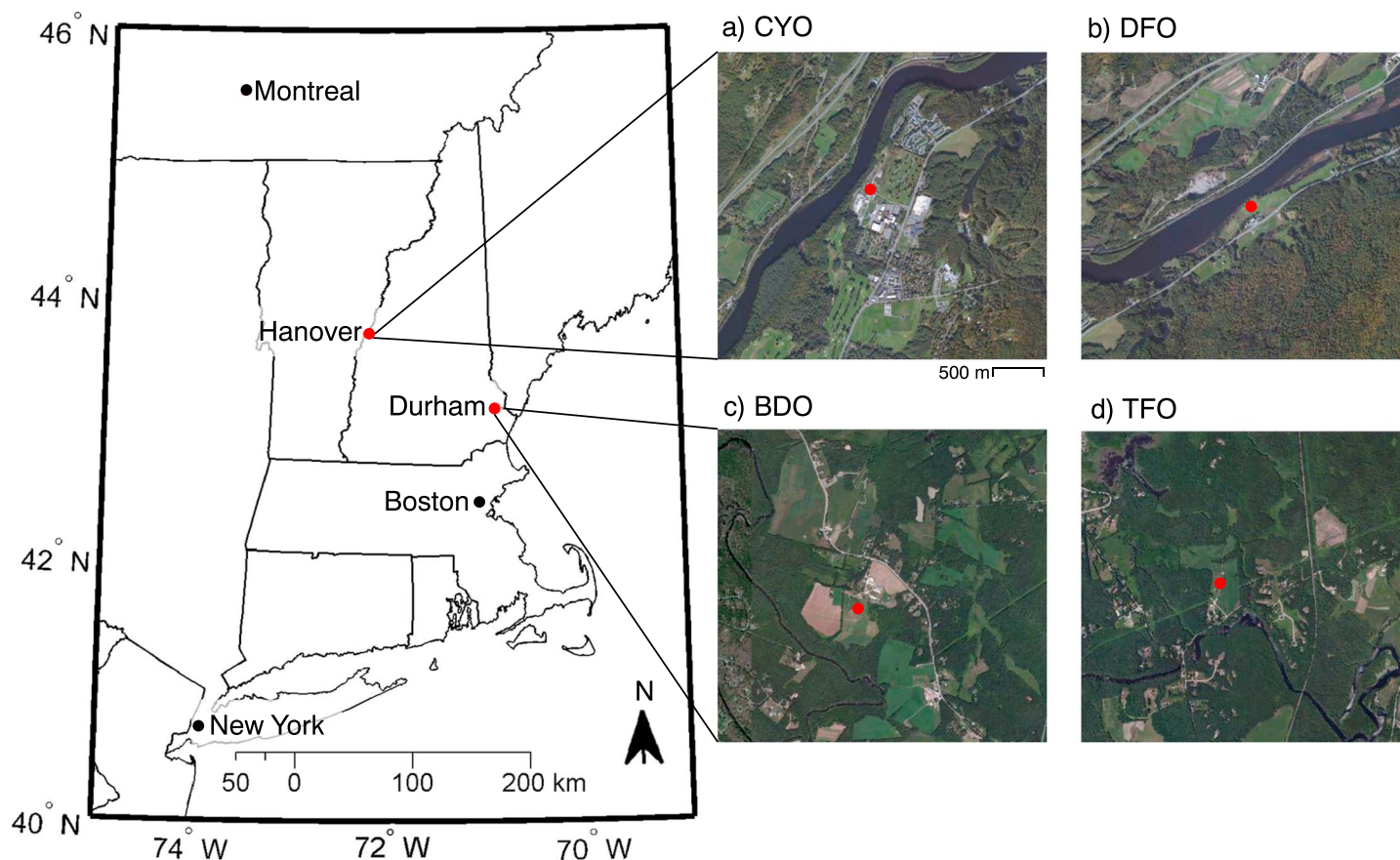
Figure 1. (left) Map of site locations indicated by red dots. (right) Satellite imagery of the sites. In Hanover (a) CRREL Yard Open site and (b) Dartmouth Organic Farm Open site. In the Durham area (c) Burley-Demerrit Farm Open site and (d) Thompson Farm Open site. All right figures share the 500 m scale bar, and red dots indicate the measurement locations in open fields.

fiber optic cable of the FieldSpec was fitted with the standard remote cosine receptor fore-optic (RCR), which integrates the incoming radiation over the hemisphere. The fore-optic rests on the end of a boom that is held at approximately 1 m above the snow surface and leveled by using a bubble level on the boom. We made paired measurements with the fore-optic pointing upward to the sky and with the fore-optic pointed downward to the snow surface. Instrument optimizations were conducted at the onset of measurement and at any noticeable lighting change. Optimization is an internal process of the instrument which adjusts gain, offset, and integration time to improve dynamic range. We collected five paired measurements each day in a single location to minimize any effect from unnoticed changes in solar conditions during measurement due to passing clouds.

After the albedo measurements, we dug a snow pit from the snow surface to the underlying soil beneath the center point of the albedo measurement. Layers within the snowpack were identified and classified by using the International Classification for Seasonal Snow on the Ground [*Fierz et al.*, 2009]. We measured snow density and snow optical grain size discretely throughout the snowpack, and collocated snow samples were collected in clean bottles for analyses of black carbon content and major ions. In 2013 and 2014, these discrete measurements were made every 3 cm starting from the surface of the snow and working downward to the snow/ground interface such that an entire vertical snow column was collected within the discrete samples. In 2015, these discrete measurements aligned with the layering from the storm events so that each sample with depth in the snow was from a given snowfall event, but again, the full depth of each layer was sampled so that an entire column of snow is collected.

We measured snow optical grain size with a spectral method developed by *Nolin and Dozier* [2000] that uses the scaled band area of the 1030 nm absorption feature in snow to determine grain size. This technique was developed for remote sensing use, and *Painter et al.* [2007a] adapted the technique to be implemented using

contact spectroscopy with an ASD FieldSpecFR and an ASD Hi-Intensity Contact Probe. We followed the same procedure outlined by *Painter et al.* [2007a], using the contact probe, which provides its own light source for the reflectance measurements. It is fitted with a dull black, dome-like spacer that blocks out incoming light and keeps the probe at a fixed distance of 1 cm. At this distance, the spot size of the instrument is approximately 2 cm. Measurements are made on the surface of the snow and down along the vertical face of the snow pit at the midpoint of each corresponding density/chemistry sample. At each location, two measurements are made rotated 180° from one another to account for any anisotropy in the grain reflectance, as the fiber optic sensor is not at nadir. Density measurements included collecting a 100 cm³ volume of snow for chemical analysis and determining the mass using a digital balance after sample collection. Samples for chemical measurements were kept frozen from the time of collection until the time of their analysis at the University of New Hampshire. Major ions were analyzed by using an ion chromatograph, and this work makes use of calcium ion concentration measurements to approximate dust concentrations in the snowpack (see further details in Text S2 in the supporting information). Black carbon analysis was done by using a Single Particle Soot Photometer (SP2), where the snow sample is melted and nebulized before analysis (see companion paper by *Lazarcik et al.* [2016] for more information regarding black carbon and ion analysis and results).

In order to put the field measurements into context of greater meteorological patterns, automatic weather stations were installed at or near the field sites. These weather stations were installed at the CRREL site in 2013–2015, at the Dartmouth Farm site in 2015, and at the Thompson Farm site in 2013–2015. The Burley-Demeritt Farm site is near enough to the Thompson Farm site that the meteorological conditions are approximately equivalent. Measurements at these stations that are included in this analysis are 2 m air temperature and precipitation amounts measured by using a heated, shielded, all-weather weighing rain gauge and an auxiliary tipping bucket [*Diamond et al.*, 2013].

2.2. Albedo Data Processing

There are a number of factors which must be considered in the accurate processing of spectral albedo data. Our albedo data processing and corrections closely follow those presented in *Carmagnola et al.* [2013] and are similar to corrections done in *Wright et al.* [2014], *Picard et al.* [2016], and *Grenfell et al.* [1994]. First, erroneous data caused by changes in cloud cover are eliminated. Because five pairs of measurements are taken each day, it is clear to see when incoming solar radiation changes rapidly and causes outliers in the spectral albedo. These outliers that stray from the otherwise repeatable measurements were removed. Additionally, any erroneous measurements that contained albedo greater than 1 or less than 0 (particularly present in bands where atmospheric water vapor is highly absorptive) were removed. After the raw data have been assured for quality, incoming solar radiation must be partitioned into diffuse and direct components, and corrections must be made to account for the solar zenith angle at measurement time, the angular response of the RCR, and the presence of the observer. These corrections follow *Carmagnola et al.* [2013], and details can be found in the Text S1. Examples of the raw albedo compared to the corrected albedo are shown in Figure S1 in the supporting information, and corrected albedo is almost always greater than or equal to raw albedo. The degree of correction depends on the fraction of incoming solar radiation that is direct or diffuse. A larger fraction of direct light results in a more significant correction factor.

After corrections have been made to the spectral albedo, further products can be derived from the data. The wavelength integrated albedo (referred to as broadband albedo hereafter) is calculated by using the corrected albedo data and the measured incoming solar radiation that is part of each albedo measurement. It is calculated as follows:

$$a_b = \frac{\int_{350}^{1850} a(\lambda) F_\downarrow(\lambda) d\lambda}{\int_{350}^{1850} F_\downarrow(\lambda) d\lambda}$$

where $\alpha(\lambda)$ is the calculated albedo at each wavelength and $F_\downarrow(\lambda)$ is the measured incoming solar radiation (as in *Perovich et al.* [2002]). Further wavelength-integrated albedos are derived to investigate visible and near-infrared (NIR) albedos independently. These are calculated by using the same equation for broadband albedo, but the limits of integration are changed. For visible albedo, we integrate from 350 nm to 750 nm, and for NIR albedo we integrate from 750 nm to 1850 nm. Though the spectrometer measures incoming radiation up to 2500 nm in wavelength, much of the data beyond 1850 nm has a signal-to-noise ratio too low to be useful.

2.3. Uncertainty Analysis

In assessing potential errors associated with grain size measurement, *Nolin and Dozier* [2000] suggest that the uncertainty of the spectral technique for grain size determination is on the order of 10–50 μm. However, *Painter et al.* [2003] present results indicating that the uncertainty may be on the order of 100 μm. Additionally, we did not cover the snowpit to prevent interference from outside irradiance, which can increase the uncertainty in the grain size measurement [*Skiles*, 2014]. Two surveys were conducted on separate days to assess the spatial variability of grain size measurement over a 20 m × 20 m grid with nine locations. Measurements were made on the snow surface with the contact probe, and a small pit was dug at each location so that measurements could be made in the top few centimeters of the vertical snow wall. On each day, variability within the survey grid was less than 15%.

Uncertainty in albedo measurements could come from a number of factors. In creating a time series of albedo measurements in which the measurement location moves, there are errors associated not only with instrument, observer, or processing uncertainties, but also with spatial variability. Using the same 20 m × 20 m grid to assess variability and one additional survey grid of 25 m × 25 m, we found that the standard deviation of broadband albedo over the survey was on average 2.1%, which is quite low (further details of survey results can be found in Table S1 in the supporting information). The five repeat measurements made every day allow us to quantify the average standard deviation of albedo within a single day. In these repeat measurements, before removing erroneous data the median and mean standard deviation of broadband albedo are 0.008 and 0.05, respectively. After the erroneous data are removed, the median and mean standard deviations are 0.008 and 0.03, respectively. Another source of uncertainty is our use of the approximation of diffuse and direct fractions of light. Independent measurements of these fractions of light would allow for more accurate corrections of the data, as done by *Carmagnola et al.* [2013], but the impacts of this approximation in lieu of measurements are not likely to be significant in this study. Another potential source of albedo reduction that is not directly addressed in this study is the presence of vegetal debris. However, our sites in open fields are as distant as possible from surrounding vegetation in order to limit this effect, and the presence of any debris is noted during field measurements. Visible debris is most common at the end of the season when the snowpack is shallow. Snowpacks less than 10 cm deep are not included in our statistical analyses.

Spatial variability of the black carbon content in the snow was determined to have a coefficient of variance of 42%, and the standard deviation of the nebulizer/SP2 was determined to be 27%. Further details of black carbon measurement uncertainty are presented in *Lazarcik et al.* [2016].

2.4. Back Trajectory Modeling

The Hybrid Single-Particle Lagrangian Integrated Trajectory (HYSPLIT) model is used to determine the trajectories of the winter storms from 2013 to 2015 [*Draxler and Hess*, 1997; *Draxler and Hess*, 1998; *Draxler*, 1999]. The model is driven with the wind vector profiles from the Global Data Assimilation System (GDAS). We determine the back trajectory of 1000 particles starting from the latitude and longitude locations of the sites at the time of snowfall, within a 3 h period (the frequency of the GDAS data). The release altitudes of the 1000 particles are distributed across a condensation profile that is determined from a lofting model. This model uses relative humidity, temperature, pressure, and vertical velocity in an iterative process where an air mass is lofted in increments and the degree of supersaturation is recalculated at each iteration and is repeated until convergence is reached. Multiplication by the vertical velocity yields the condensation rate. The MATLAB program which executes the lofting model and interfaces with the NOAA HYSPLIT model was developed by *Putman* [2013], and further details of the lofting model can be found therein.

Winter storms in New Hampshire have a tendency to follow one of three common trajectories: (a) storms that move across the northern continental United States (Land), (b) storms that come up the eastern seaboard of the United States (Coast), and (c) storms that move inland from the Atlantic Ocean (Sea). Prototypical cases of each storm type are shown in Figure 2. Each of the storms considered from 2013 to 2015 is categorized into one of these groups based on the number of discrete back trajectory points that fall within the relevant locations of the storm types. Further details about storm groupings can be found in Text S3.
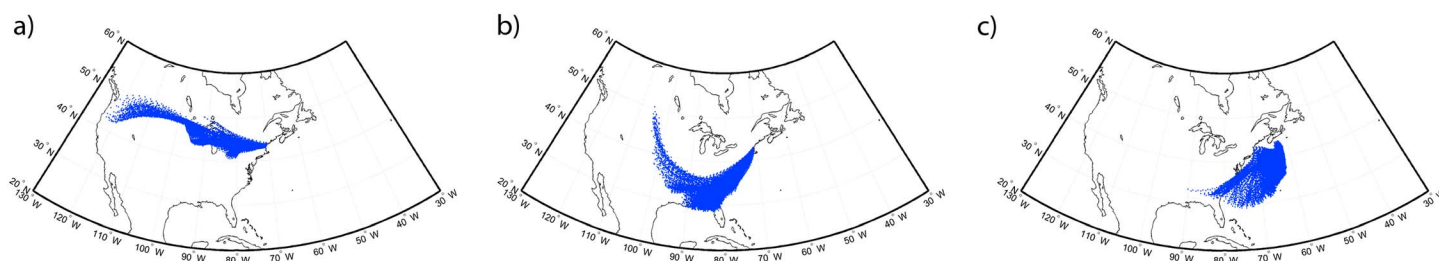
Figure 2. HYSPLIT back trajectories for three types of winter storms experienced in New Hampshire: (a) land-based storms from across the northern continental U.S. (Land), (b) storms that come up the eastern seaboard (Coast), and (c) storms that move inland from the Atlantic Ocean (Sea). These different storms track moisture from different locations and bring in different types of air masses, and thus are expected to result in different types of snow.

3. Results

The 3 years of this study represented a significant fraction of the range of temperature conditions and snowfall amounts that have been experienced in the New England area over the past several decades. Year 2013 was a relatively warm winter, as indicated by the average temperature in Hanover and Durham from January through March (Table 2). There was relatively little snow that year as well. The winter of 2014 was colder than 2013, and 2015 was even colder. Hanover is consistently colder than Durham due to its higher latitude, higher altitude, and distance from the coast. In 2014, the maximum snow depth in Hanover (63 cm) was significantly higher than in Durham (45 cm); in 2015 the opposite was true (Table 2). The number of precipitation events varied year to year (Table 2), with 2015 having the most frequent events at both sites. HYSPLIT analysis reveals that storm paths differed for the two towns (Table 2). In the 3 years of the study, Hanover received 59% Land storms, 30% Coast storms, and only 11% Sea storms. In Durham, the divisions between Land, Coast, and Sea storms were 28%, 41%, and 31%, respectively. On average, Land-based storms had a median transit time of 43 h from the time they leave the planetary boundary layer, and Coast and Sea storms had median transit times of 16 h and 11 h, respectively. Having data from these different sites in years that exhibited such different meteorological conditions provides a range of conditions for us to study the evolution of snow albedo.

Temperature and storm frequency strongly impact the snow albedo through their controls on snow depth and snow metamorphism. Figures 3–5 show broadband albedo over the 3 years at all three sites. In 2013, the snowpack was completely depleted multiple times early in the season at Hanover and Durham sites. After day 40 the albedo remained fairly low, only rising significantly to about 0.8 on one occasion, perhaps partially due to the fact that the snowpack was optically thin for much of March. Additionally, all snow was depleted before the end of March at all three sites. In 2014, each site had significantly more snow; there was continuous snow coverage at the Hanover site and only one snow depletion event at each of the Durham sites, which occurred in mid-January. However, there were still distinct periods of brief but continuous decline in albedo throughout the 2014 season (days 26–34 and days 49–53), when differences between the Hanover and Durham sites become more noticeable. The albedo decline at the Durham sites is likely more pronounced than at the Hanover sites due to more rapid grain growth in higher temperatures. The snowpack persisted at CRREL Yard Open (CYO) more than 10 days longer than at the Durham sites because of a combination of lower temperatures and a higher rate of snowfall (Table 2). The winter of 2015 was colder and saw consistently high albedo throughout the bulk of the season. An unfortunate gap in albedo data exists in the Durham records between days 21 and 41. We know from daily observations that there was a brief depletion of snow at the Durham sites followed by significant snowfall events in late January and early February. Durham received more snow than Hanover, but because Hanover is colder, the snowpacks were depleted at the end of the season on the same day.

Our mean measured surface grain size across all sites, and field seasons is 104 μm, with a standard deviation of 75 μm, a maximum of 400 μm and minimum of 10 μm. Using the same technique, *Painter et al.* [2007a] report grain sizes between approximately 80 μm and 2000 μm in the San Juan Mountains and grain sizes between approximately 40 to 400 μm at Swiss Camp in Greenland. *Nolin and Dozier* [2000] report grain sizes between 60 and 700 μm from several locations in the U.S. and Greenland.

Over all three seasons and sites, measured surface black carbon concentrations have a mean of 10 ppb, with a standard deviation of 9.8 ppb, a minimum below detection limit and a maximum of 97 ppb. The distribution is

Table 2. Summary of Basic Meteorological Parameters for Two Site Locations Over the Range of Study Years[a]

Site	Year	Mean Temperature (January–March)	Max. Snow Depth	Number of Precipitation Events (January–March)	Percentage of Land Storms	Percentage of Coast Storms	Percentage of Sea Storms
Hanover	2013	−3.1°C	25 cm	22	52%	36%	12%
	2014	−6.9°C	63 cm	17	32%	47%	21%
	2015	−8.7°C	49 cm	27	85%	11%	4%
Durham	2013	−1.7°C	27 cm	21	12%	44%	44%
	2014	−4.6°C	45 cm	26	20%	50%	30%
	2015	−6.3°C	62 cm	31	43%	32%	25%

[a]Months included in this analysis are January, February, and March because they make up the bulk of our measurement season each year. Precipitation events include all types of precipitation in excess of 2 mm water equivalent in a day.

skewed low, such that 75% of surface measurements are below 13 ppb. In eastern Sierra Nevada, mean black carbon concentrations were 25 ppb during the accumulation period and 135 ppb during ablation [*Sterle et al.*, 2013]. *Doherty et al.* [2014] measured black carbon content in a survey of sites across western and central North America and found concentrations that were typically between 5 and 70 ppb. Through measurements in Idaho and Utah, *Doherty et al.* [2016] found black carbon concentrations ranging from 4 to 45 ppb, but significantly more light-absorbing impurities in the snowpack that were attributed to dust and soil. Concentrations of black carbon measured in New Hampshire fall within the range of those measured across North America, but are on the lower end.

Conservative estimates of dust concentration in the New Hampshire snowpacks yield mean dust concentrations between 0.2 and 1 ppm, with minimum values below detection limits and an overall one time maximum
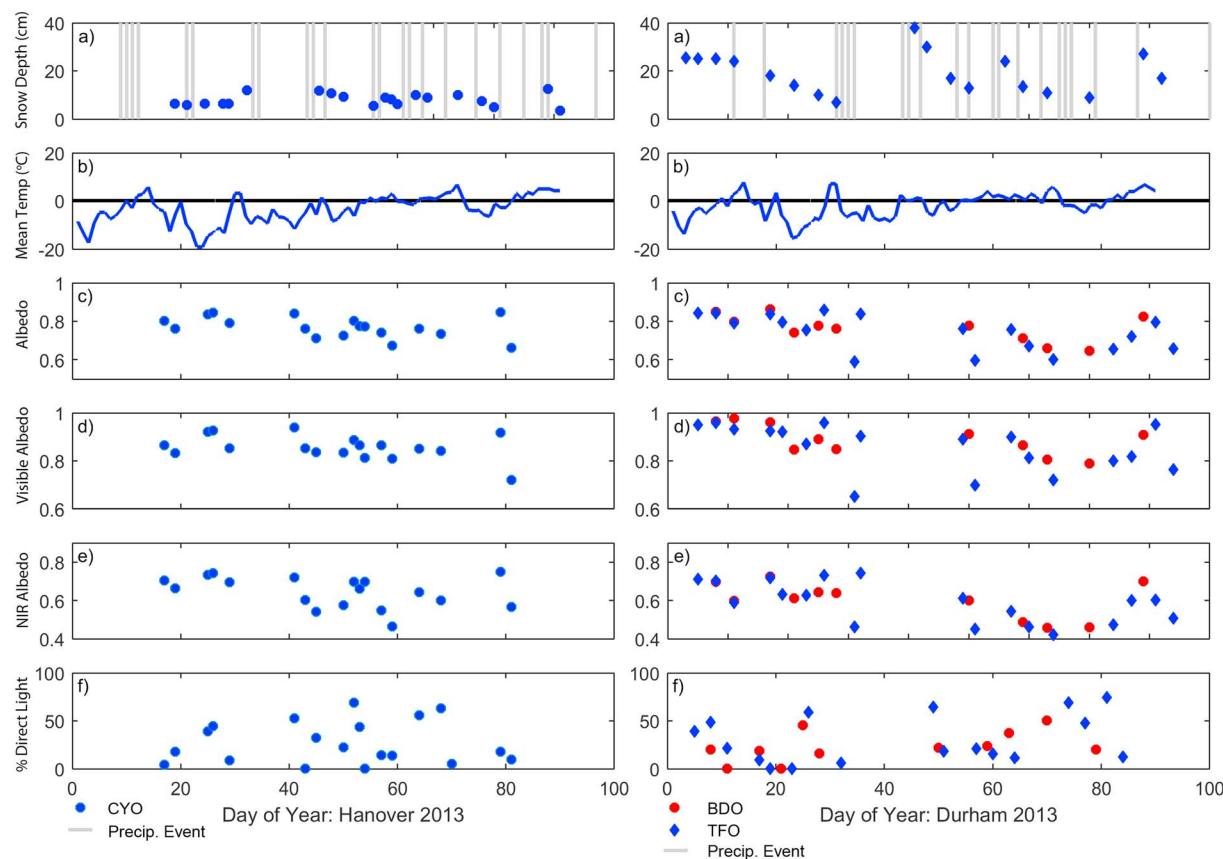

Figure 3. Time series data shown for all three sites in 2013, with the Hanover site on the left and Durham sites paired together on the right. For each site/year combination, we present (a) snow depth (cm) with gray lines indicating precipitation events, (b) mean air temperature (°C), (c) broadband albedo (350–1850 nm), (d) visible albedo (350–750 nm), (e) near-infrared albedo (750–1850 nm), and (f) percent of incoming illumination that was direct (calculated by using formulas from *Weiss and Norman* [1985], see details in Text S1).
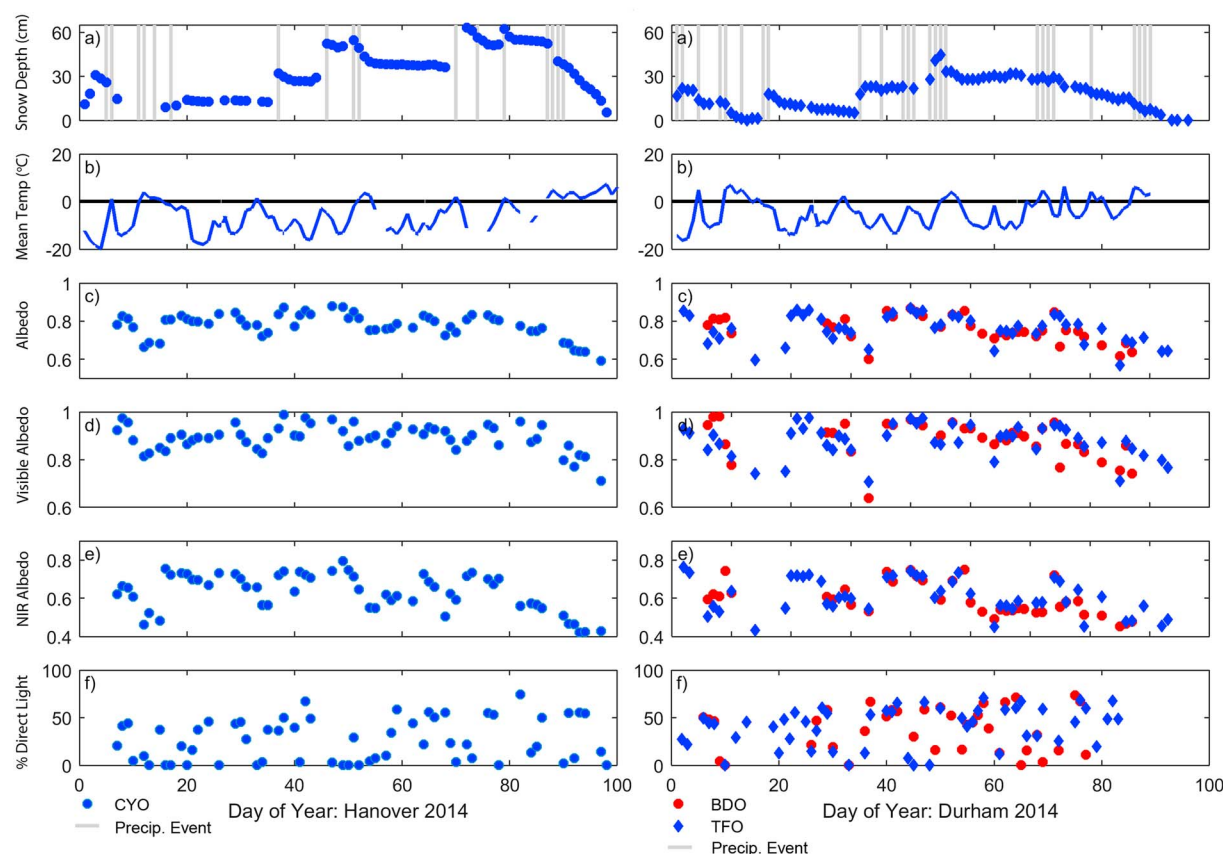
Figure 4. Time series data shown for all three sites in 2014 as in Figure 3.

of 27 ppm (detailed results in Table S2). These concentrations fall well below studies in regions where dust plays a significant role in albedo. In the mountains in the western U.S., concentrations of 370 ppm on average were found in the San Juan Mountains [*Painter et al.*, 2007a], and concentrations of 830–4800 ppm were reported in the Colorado River Basin [*Skiles et al.*, 2015]. In Nepal, *Kaspari et al.* [2014] report concentrations of 9300 ppm. In Greenland, however, average concentrations as low as 0.064 ppm have been reported [*Polashenski et al.*, 2015]. As may be expected, dust concentrations in New Hampshire are much lower than in dry regions of the western United States and Nepal but are higher than in remote locations such as Greenland that are much further from any sources of dust.

Example spectral albedo plots that represent different snow and lighting conditions are shown in Figure 6. The grain size has a clear impact on the spectral albedo, where larger grains result in lower albedo, particularly in the near infrared. The impact of lighting conditions is also shown. Refer to Figure S2 for an example of the profile of snow properties measured each day and to Figure S3 for an example of the evolution of snow albedo over several days.

To analyze the evolution of the albedo throughout the three winter seasons at each of the sites, we will first investigate the physical and chemical properties of the snow when it is freshly fallen. Each fresh snow event creates a local maximum in the albedo record, though the albedo of fresh snow is not constant. As the snowpack continues to develop through grain metamorphism, impurity loading, and redistribution processes, there are significant declines in albedo. We will investigate the main drivers of this albedo reduction in the New Hampshire snowpacks.

4. Properties of Fresh Snow

We anticipated that the physical and chemical properties of the snow resulting from varying storm trajectories would differ, and the variability of storm types in New Hampshire (Figure 2) allowed us to explore this
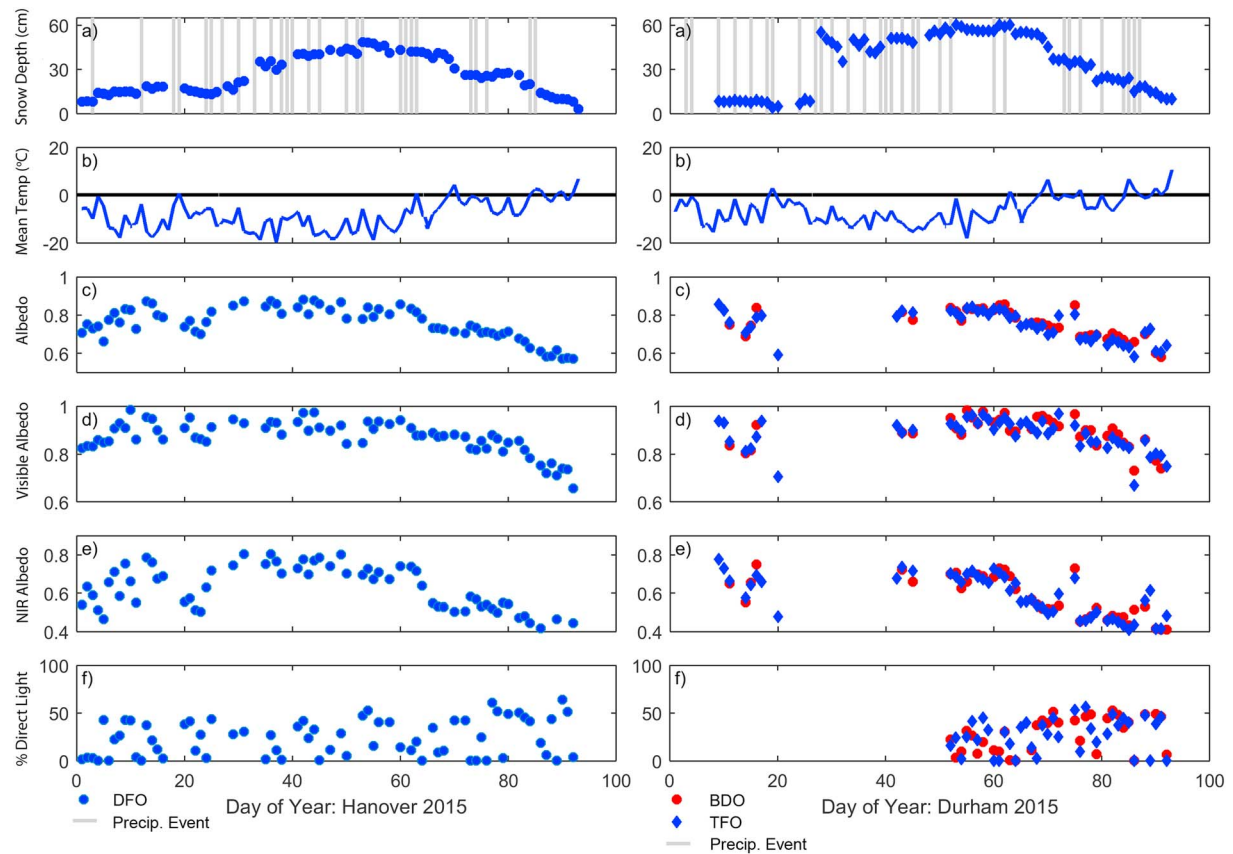
Figure 5. Time series data shown for all three sites in 2015 as in Figure 3.

hypothesis. In particular, we hypothesized that Coast and Land storms may have higher impurity content than the Sea storms because of their trajectories over major metropolitan and industrial areas, which are sources of black carbon. In the analysis of the storm trajectories, storms from 2013 to 2015 at all sites were included so long as we had corresponding field measurements within 24 h of the snowfall event. This was almost always the case in 2014 and 2015 because of near daily sampling, but some storms were missed in 2013 due to lower frequency field measurements.

Using Tukey-Kramer tests to analyze differences in mean properties from each storm type [*Tukey*, 1949], we find that the path of a storm impacts some snow properties significantly. Means and standard error of these storm snow properties are shown in Figure 7, and significance results from the Tukey-Kramer tests are shown in Table 3. There is a significant impact of storm type on the black carbon content, with Coast storms having higher black carbon content than the Sea storms and Land storms (Figure 7). Optical grain size tends to be slightly smaller in Sea storms, but there is only a weakly significant difference to the Coast storms and none to the Land storms. Resulting differences in the snow albedo are only marginally significant. Land storms result in a higher mean snow albedo than the Coast and Sea storms in the near-infrared and visible ranges, respectively. Land storms have an albedo that is higher than Sea storms by 0.04 in the visible, and higher than Coast storms by 0.04 in the NIR. However, these results only show a weak significance. Interestingly, we might hypothesize that Land storms may have higher albedo because they deposit the most fresh snow, but it is not the case. Land storms bring the least amount of precipitation (see Table 3 and Figure 7).

We propose that the difference in albedo is potentially driven by the cloud temperature where the snow crystals are formed and the air temperature post deposition, both of which impact the snow structure and ultimately the snow albedo. Temperatures at the heights of particle release (chosen to coincide with cloud decks) were extracted from the GDAS data set and indicate that the cloud temperature of Land storms is on average $-27 \pm 15°C$ (error bars in this case and hereafter refer to one standard deviation), whereas cloud
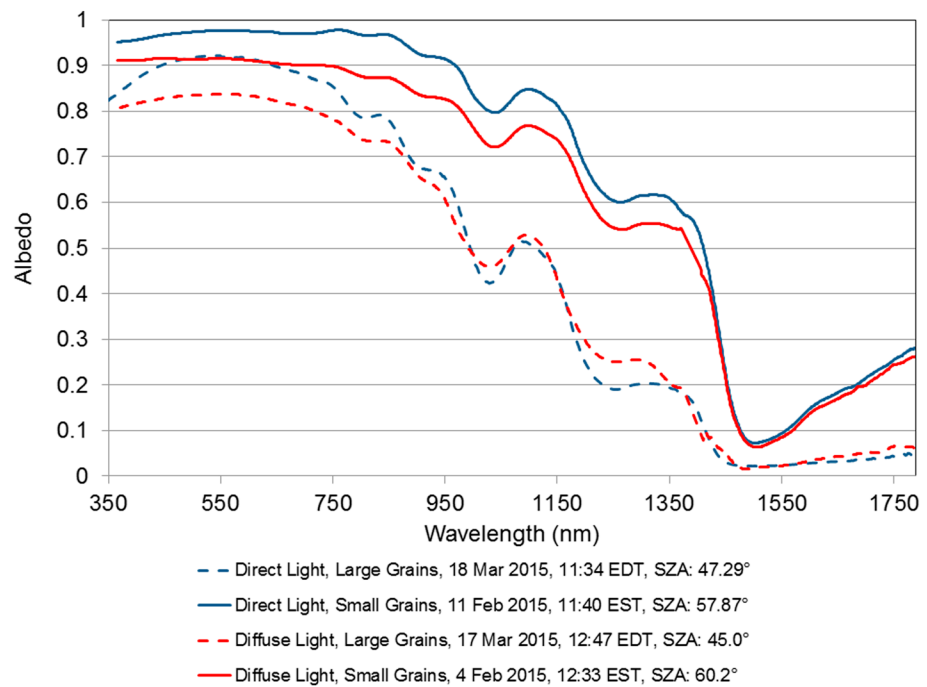
Figure 6. Example spectra of snow representing different snow conditions and lighting conditions. Intrinsic properties of the snow such as the grain size and impurities and external factors, such as illumination, impact the resulting spectral albedo.

temperatures for the Coast and Sea storms are significantly higher, $-16 \pm 9°C$ and $-14 \pm 8°C$, respectively (Figure 7). Differences in temperature are accompanied by similar differences in cloud height, with Land storms that have an average initial cloud height of 525 ± 176 mbar, and Coast and Sea storms that have average initial cloud heights of 624 ± 125 mbar and 697 ± 132 mbar, respectively. The weather station data indicate that air temperature accompanying Land and Sea storms is on average lower ($-5.5 \pm 4.7°C$ and $-5.3 \pm 5.4°C$, respectively) than the Coast storms ($-3.8 \pm 4.4°C$), with only the difference between Land and Coast storms being marginally significant in our Tukey-Kramer analysis of means. There is an established link between the temperature and supersaturation conditions and the resulting crystal formation [*Hallett and Mason*, 1958], so the difference in temperature in the storm cloud decks could result in structural differences in snow grains. Crystals continue to develop and aggregate as they fall through the atmosphere [*Libbrecht*, 2005]. During their descent, the temperature and supersaturation conditions are subject to change. Land storms have a significantly colder snow formation temperature, but a ground-based air temperature within a few degrees of the other storm types. Therefore, Land storm snow grains are subjected to the largest variety of temperature conditions as they fall from the atmosphere. Being subjected to a number of different temperature and supersaturation conditions may lead to several different types of growth patterns within one snow grain and therefore result in a more complex crystal [*Hallett and Mason*, 1958]. This increased complexity, with more air ice interfaces, might lead to a higher albedo. Unfortunately, it is difficult to consistently discern grain types of the fresh precipitation due to rapid grain development after deposition. Often, by the time of observation, even if it is merely hours after the snowfall, the precipitation particles have become fragmented and no longer retain their initial shape. In particular, the higher air temperatures that accompany Coast storms may result in an increased rate of metamorphism, which is a temperature sensitive process [*Colbeck*, 1982]. This would result in reduced grain complexity and lower snow albedo as compared to Land storms that coincide with lower air temperatures and slower metamorphism rates. We analyzed the average time between peak snow deposition and subsequent snow measurements for the data used in this analysis and found that there was no significant difference based on storm type, so while it will impact individual measurements, the data should not be biased by the time delay between deposition and measurement. Initial snow albedo immediately postdeposition is important, as the structure of fresh snow yields the highest albedo, only declining as the snow metamorphoses.
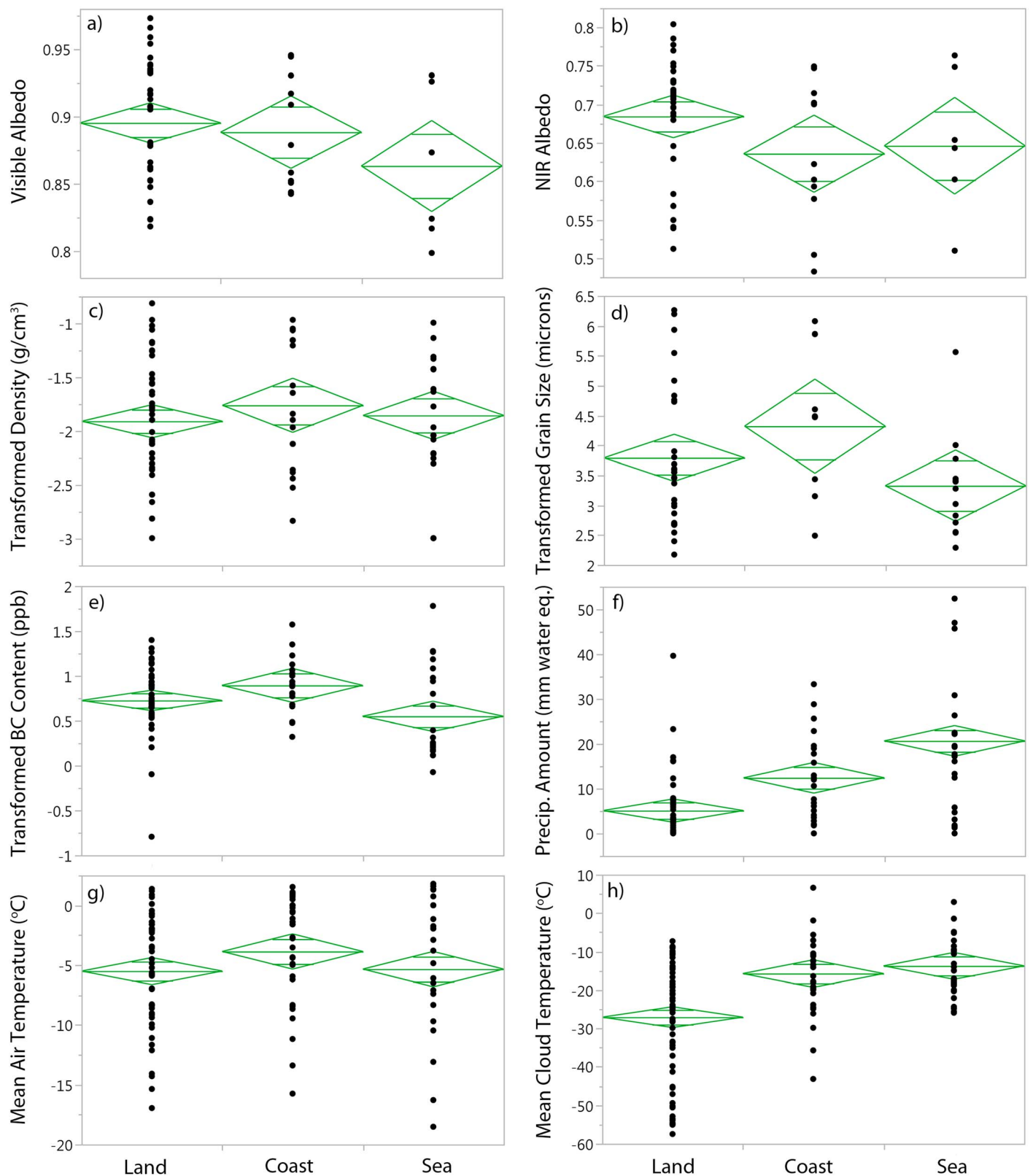
Figure 7. Snowpack and atmospheric parameters including (a) visible albedo (350–750 nm), (b) near-infrared albedo (750–1850 nm), (c) log-transformed density (g/cm^3), (d) cube-root transformed grain size (μm), (e) log-transformed black carbon content (ppb), (f) precipitation amount (mm water eq.), (g) mean air temperature (°C), and (h) mean cloud temperature (°C) are categorized based on the path of the winter storm event, defined as either Land-, Coast-, or Sea-based. All measurements made within 24 h of snowfall.

Table 3. Means of Snow Properties From Different Storm Types and Results From Tukey-Kramer Method of Comparing Means[a]

	Land	Coast	Sea
Albedo (Visible)	**0.90**	0.89	**0.86**
Albedo (NIR)	**0.68**	**0.64**	0.65
Atmospheric temperature (°C)	**−27***	**−16***	**−14***
Air temperature (°C)	**−5.5**	**−3.9**	−5.3
Black carbon content (ppb)	**6.9**	**9.6***	**7.4***
Optical grain size (μm)	140	**198**	**88**
Snow density (g/cm^3)	0.17	0.20	0.18
Precipitation (mm–water eq.)	**5.1***	**12.4***	**20.7***

[a]Pairwise tests were conducted after significant analysis of variance tests revealed differences in the means. Significant tests are bolded with an asterisk ($p < 0.05$), and marginally significant tests ($p < 0.2$) are only bolded. A significant test indicates that the means of the two storm types indicated by the column are significantly different.

5. Snow Albedo Evolution

Snow albedo is largely driven by the presence of impurities in the visible range and by the size of the snow grains in the near infrared range; however, this simple framework is complicated by the fact that larger grains amplify the impacts of impurities in the visible range, and higher impurity content can impact NIR albedo [*Hadley and Kirchstetter*, 2012]. We trace the evolution of the snow albedo throughout the winter seasons in Figures 3–5, plotting not only broadband albedo, but also visible and NIR albedo. Because grain size and black carbon content reduce albedo in different parts of the spectrum, this allows us to determine the drivers of albedo in this geographic region. In New Hampshire, where winter temperatures are often just below freezing, snow is subject to relatively rapid metamorphism. There is often a concurrent rise in albedo as snow depth increases due to fresh snowfall. Snow events cause "freshening" and blanket the older snow with a surface layer of new, smaller grains that increase the albedo. Clear examples of this can be seen in Figure 4 in the Hanover 2014 record, e.g., days 36 and 72. We can also see a link between increased air temperature and a sharp decline in snow albedo, particularly in the near-infrared (e.g., Figure 4, Hanover 2014: days 32 and 53; Figure 5, Hanover 2015: days 5 and 65). This phenomenon can be explained in two ways: by accelerated snow metamorphism that occurs as temperature increases producing larger, typically rounded grains and clusters, and by snowmelt. When the snow temperature reaches 0°C, albedo declines rapidly, as the snowpack is no longer evolving through isothermal or temperature gradient metamorphism [*Colbeck*, 1982; *Flanner and Zender*, 2006], but through phase changes from ice to water. Meltwater can refreeze at the surface forming crusts or percolate and refreeze at lower levels in the pack when temperatures decrease at night or in following days. The resulting forms from the melt/refreeze pattern are hardened crusts made up of aggregated rounded grains and clusters of grains that have frozen together. The grains and clusters are more or less discernable depending on the extent of the melt before refreeze. Melt/freeze forms are common in the New Hampshire snowpack. Rapid grain growth caused by higher temperatures and the melt and refreeze patterns of snow both reduce albedo. During periods of consistently low temperatures, we observe that fresh snowfall quickly becomes fragmented precipitation particles, but then evolves much more slowly. In cold conditions, these grains only become rounded or faceted after significant time exposed at the surface, often being buried by fresh snow before this evolution can occur. In the end of the season, larger rounded grains and grain clusters are common at the surface, as grain metamorphism is occurring rapidly in the warmer conditions.

While the winter of 2014 was quite cold on average (Table 2), there was significant variability in the air temperature (Figure 4). These fluctuations, combined with the proximity of the air temperature to the freezing point, led to marked changes in albedo throughout the season, particularly evident in the near-infrared part of the spectrum. On the contrary, the winter of 2015 had a long period of time where temperatures were consistently below freezing (approximately day 25 through day 65), and snow events were occurring regularly (Figure 5 and Table 2). The combination of low temperatures and consistent snowfall led to constantly high albedo during that time in both visible and NIR ranges, with the overall broadband albedo having a standard deviation of less than 0.04 in that forty day window.

Grain size is driving variability in albedo, as changes in NIR albedo are so large and concurrent with changes in temperature and timing of snow events, which strongly affect grain size. To test the relative impact of grain
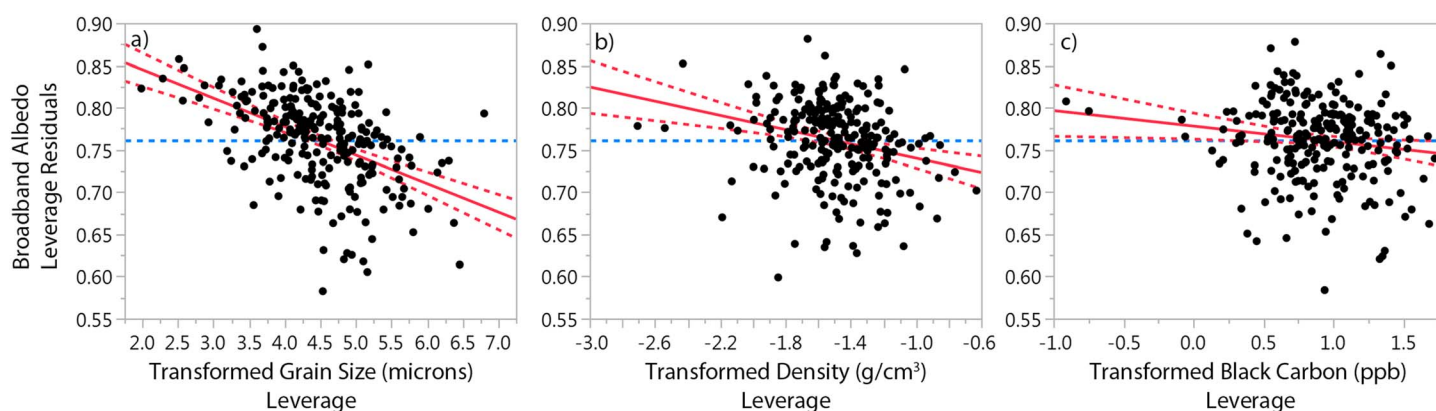
Figure 8. Multiple linear regression leverage plots [e.g., *Sall*, 1990] from prediction of broadband albedo based on the surface optical grain size (μm), surface density (g/cm^3), and the surface black carbon content (ppb) in the top 5 cm of snow for all three sites in 2013–2015. Variables are transformed to create a normal distribution. The combination of variables describes 58% of the variance in broadband albedo ($p < 0.0001$). Transformed optical grain size, density, and black carbon account for 45% ($p < 0.0001$), 10% ($p < 0.0001$), and 3.2% ($p = 0.0222$) of the variance, respectively. Similar analyses for visible and NIR parts of the spectrum are shown in Figures S4 and S5.

size, density, and black carbon content on broadband albedo, multiple linear regression analysis was conducted by using data from all sites in 2013–2015 when the snowpack was greater than 10 cm. Measurements of the three independent variables are taken from any sample within the top 5 cm of snow. In most cases, this includes an average of two measurements of each variable. This type of regression allows us to determine the magnitude of the independent effect of each explanatory variable when other variables are held constant. For the multiple linear regression, all variables are transformed in order to attain a normal distribution, which is a required assumption of linear regression. Black carbon content and density are log-transformed, and grain size is transformed with a cube root to meet this criteria. The regression is significant (Figure 8), with 45% of variability in broadband albedo explained by the optical grain size parameter, 10% explained by the density parameter, and only 3.2% explained by the black carbon content parameter. While the fraction of variability explained by black carbon is low, this does not mean that the presence of black carbon is not reducing the snow albedo; any quantity of black carbon will cause some reduction of snow albedo [*Warren and Wiscombe*, 1980; *Hadley and Kirchstetter*, 2012]. However, the lack of correlation does indicate that in the NH snowpack black carbon is a minor factor in albedo decline. Indeed, we even see that though black carbon can be somewhat enhanced in the surface at the end of the season [see *Lazarcik et al.*, 2016], we do not find a strong correlation between albedo and black carbon content then, as grain size dominates these changes in albedo.

We compare these findings to the SNICAR model [*Flanner et al.*, 2007] through a Monte Carlo style simulation by using the MATLAB version of SNICAR. We ran 1000 iterations of the model allowing a number of variables to be randomly assigned a value between maximum and minimum values that correspond to our field measurements. The variables that were assigned this way were grain size, black carbon content, snow density, snow depth, solar zenith angle, and direct or diffuse lighting conditions. Inputs to the model can be found in Table S3. Other variables were left to default settings. We then use the paired input parameters and output broadband albedo to conduct the same multiple linear regression analysis that was done with our field measurements with grain size, black carbon, and density as independent variables. In this way, we can compare the sensitivities in the SNICAR model to the sensitivities that we find in the measurements (see Table 4). We conduct the multiple linear regression on the SNICAR output because in the model itself, sensitivities to grain size, density, and black carbon content are the result of a physical model of radiative transfer, not empirically determined values. We find that in the SNICAR-produced data set, 69% of variability can be explained by the combination of grain size, density, and black carbon, but almost all of the variability is explained by grain size (68.5%). Only 0.5% of the variability is explained by the black carbon content and snow density does not significantly account for any amount of variability explained. We also find that the regression of our data indicates a higher sensitivity to grain size than that of the SNICAR data. The coefficient paired with the grain size parameter is −0.034 in our multiple linear

Table 4. Results of Comparison Between Multiple Linear Regressions of Measured Values and of SNICAR Generated Data Set[a]

Data Set	R^2 Value[b]	Grain Size Effect		Black Carbon Effect		Density Effect	
		Sensitivity[c]	% of Variability Explained	Sensitivity[c]	% of Variability Explained	Sensitivity[c]	% of Variability Explained
In situ measurements (this work)	0.58	−0.034	45%	−0.018	3.2%	−0.042	10%
SNICAR Monte Carlo simulation	0.69	−0.028	68.5%	−0.003	0.5%	0.004	–

[a]Regression of transformed grain size, black carbon, and density to predict broadband albedo (350–1850 nm).
[b]R^2 value indicates the fraction of variability in the albedo that is described by the three parameters in this multiple linear regression (grain size, black carbon, and density).
[c]Sensitivity indicates the coefficient of each variable in the multiple linear regression to predict broadband albedo.

regression, and it is −0.028 for the SNICAR data set (Table 4). Sensitivities to black carbon content and density are also higher for our data than the SNICAR data set. These differences could be a result of a larger number of uncontrolled variables in our measurements. Additionally, uncertainty in measurements of grain size may also explain this discrepancy. It is also possible that these differences indicate that albedo sensitivities in the SNICAR model do not work perfectly in this region. This is only a pilot comparison, and in depth comparisons between SNICAR and our spectral albedo and layered snow measurements will be the subject of future work.

6. Albedo Parameterization

Because snow albedo in this region is mainly driven by the grain size, we now parameterize the albedo using easily accessible metrics that are linked to processes 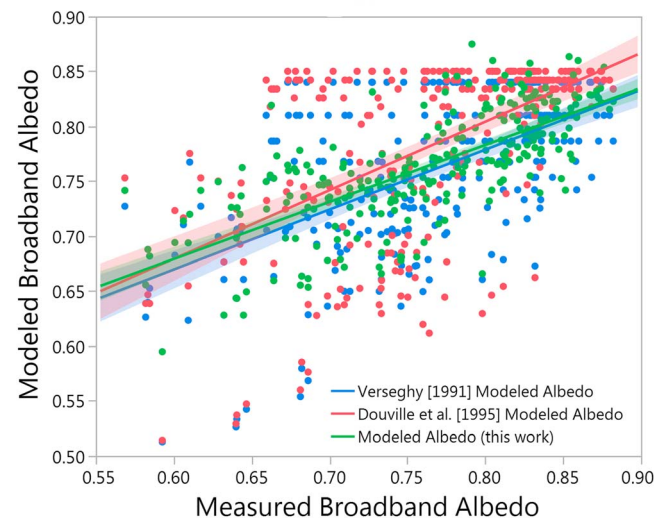of grain growth. As seen in the discussion of Figures 3–5, two important parameters are the frequency of fresh snowfall and the air temperature. Specifically, we use the number of days since snowfall as a metric to account for the amount of time that snow has been aging on the surface of the pack, and we use the mean air temperature since last snowfall as a metric to account for the rate of snow metamorphism, which is sensitive to temperature. This analysis incorporates data from all sites in 2014–2015 on days when the snow depth was greater than 10 cm. We calculate an R^2 value of 0.52 by using a multiple linear regression that includes the number of days since snowfall and the mean air temperature (see Figure 9). This indicates that in a fairly clean snowpack, over half of the variability in broadband albedo can be accounted for using two metrics that are fairly accessible in areas with meteorological

Figure 9. Multiple linear regression using mean daily temperature and days since snowfall to predict broadband albedo. Modeled albedo is calculated as follows: Broadband albedo = 0.736 − (0.0080 * Mean Temp. (°C)) − (0.006 * Days since Snowfall). This figure compares the predicted albedo by using this regression to two other models found in the literature, the *Verseghy* [1991] model and the *Douville et al.* [1995] model, that also use days since snowfall and temperatures. Because our model was used to generate the linear regression model, it yields the best fit, with an R^2 of 0.52, where the *Verseghy* and *Douville et al.* models have R^2 values of 0.25 and 0.26, respectively.

monitoring. The resulting equation is as follows:

$$\text{Broadband albedo} = 0.736 - (0.0080 * \text{Mean Temp. (°C)}) - (0.0060 * \text{Days since Snowfall})$$

Analysis was tested with maximum daily air temperature since snowfall, and the resulting R^2 value was 0.39. While the amount of variability that is explained by using this regression is only about half of the actual variability in albedo, implementation of even this simple regression could improve snow forecasting when explicit physical albedo models such as SNICAR are not used. We compare our parameterization to two other albedo decay curves that also use days since snowfall and temperature parameters (see Figures 9 and S6), a model by *Verseghy* [1991] developed for the Canadian Land Surface Scheme for global circulation models and a model by *Douville et al.* [1995] for the Météo-France climate model. While our parameterization describes 52% of the variability in the data, the *Verseghy and Douville et al.* models only describe 25% and 26%, respectively. This is not surprising, given that our parameterization was developed specifically for these sites, while these models from the literature are meant to be used globally. These models underpredict the few highest albedos, but their main deviance from our data occurs due to the assumption of a fixed value for the albedo of fresh snow. Because snow grains can change so rapidly in higher temperatures, our data suggest that models should include a temperature dependence of the albedo of fresh snow. Unfortunately, we do not have the required suite of in situ measurements to compare our parameterization to more recent albedo decay curves that require snow temperature gradient data, such as the parametrizations described in *Flanner and Zender* [2006] implemented in newer versions of the National Center for Atmospheric Research Community Land Model [*Oleson et al.*, 2010].

Our parameterization based on temperature and time since snowfall has limitations as a result of the assumptions of linearity and the dependence on only temperature and days since snowfall. A linear dependence on temperature can only work for a fixed range of temperatures, as it would yield a model albedo above 1 at very low temperatures. As a result, this model would not work in climates significantly colder than New Hampshire. Additionally, albedo can only be best parameterized this way when impurities do not play a significant role, as we have shown in our analysis of New Hampshire snow. If a system is dominated by the presence of light-absorbing impurities such as dust or black carbon [e.g., *Doherty et al.*, 2016], then our parameterization, which focuses on the impact of grain growth on albedo, would not be sufficient.

However, precipitation and temperature are two of the most important climatological variables and are both projected to be impacted by changing climate with increasing temperatures and larger variability in precipitation [*Intergovernmental Panel on Climate Change*, 2013]. Therefore, understanding the sensitivity of snow albedo to these parameters in this region is critical not only because the parameters are easily accessible, either through measurements or models, but also because they are certain to change over the next several decades. The parameterization we present may be useful, if implemented, to better represent snow albedo in short-term seasonal snow forecasting or in longer-term climate modeling in cases where snow grain size and impurity loading information for physically based albedo models is not available.

7. Conclusions

This work presents the first detailed measurements of the evolution of seasonal snow albedo, black carbon, and physical characteristics of snow through several New Hampshire winters. We have discovered that the albedo of fresh snow is marginally sensitive to the path of the winter storm, and this sensitivity is potentially caused by differences in grain morphology due to cloud temperature at snow crystal formation. As snow ages, changes in broadband albedo are driven by changes in grain size. In contrast to publications from other areas of the U.S. and Greenland, we have found that dust exists in such low quantities that it has no impact on snow albedo and black carbon plays only a minor role in the seasonal evolution of snow albedo in New Hampshire. Black carbon does reduce albedo, but, at the concentrations measured in this region, the changes are not significant compared to changes driven by grain size. Grain size evolution is controlled by metamorphism and storm frequency, but we note that the presence of black carbon and other light-absorbing impurities may accelerate grain growth and is worth further investigation. We have presented a new parameterization of albedo based on temperature and days since snowfall, variables that are linked to metamorphism. Our improved understanding of current controls on snow albedo in this region allows us to assess potential impacts of future changes anticipated in the winter seasons to the snowpack. Continued research will focus on linking projected regional climate changes to the resulting snow albedo.

References

Aoki, T., T. Aoki, M. Fukabori, A. Hachikubo, Y. Tachibana, and F. Nishio (2000), Effects of snow physical parameters on spectral albedo and bidirectional reflectance of snow surface, *J. Geophys. Res.*, *105*, 10,219–10,236, doi:10.1029/1999JD901122.

Aoki, T., A. Hachikubo, and M. Hori (2003), Effects of snow physical parameters on shortwave broadband albedos, *J. Geophys. Res.*, *108*(D19), 4616, doi:10.1029/2003JD003506.

Aoki, T., H. Motoyoshi, Y. Kodama, T. J. Yasunari, and K. Sugiura (2007), Variations of the snow physical parameters and their effects on albedo in Sapporo, Japan, *Ann. Glaciol.*, *46*(1), 375–381, doi:10.3189/172756407782871747.

Aoki, T., K. Kuchiki, M. Niwano, Y. Kodama, M. Hosaka, and T. Tanaka (2011), Physically based snow albedo model for calculating broadband albedos and the solar heating profile in snowpack for general circulation models, *J. Geophys. Res.*, *116*, D11114, doi:10.1029/2010jd015507.

Banta, J. R., J. R. McConnell, R. Edwards, and J. P. Engelbrecht (2008), Delineation of carbonate dust, aluminous dust, and sea salt deposition in a Greenland glaciochemical array using positive matrix factorization, *Geochem. Geophys. Geosyst.*, *9*, Q07013, doi:10.1029/2007GC001908.

Barnett, T. P., J. C. Adam, and D. P. Lettenmaier (2005), Potential impacts of a warming climate on water availability in snow-dominated regions, *Nature*, *438*(7066), 303–309, doi:10.1038/nature04141.

Brown, R. D., and P. W. Mote (2009), The response of northern hemisphere snow cover to a changing climate*, *J. Clim.*, *22*(8), 2124–2145, doi:10.1175/2008jcli2665.1.

Burakowski, E. and M. Magnusson (2012), Climate impacts on the winter tourism economy in the United States, Natural Resources Defense Council.

Carmagnola, C. M., et al. (2013), Snow spectral albedo at Summit, Greenland: Measurements and numerical simulations based on physical and chemical properties of the snowpack, *Cryosphere*, *7*(4), 1139–1160, doi:10.5194/tc-7-1139-2013.

Cohen, J., et al. (2014), Recent Arctic amplification and extreme mid-latitude weather, *Nat. Geosci.*, *7*(9), 627–637, doi:10.1038/ngeo2234.

Colbeck, S. C. (1982), An overview of seasonal snow metamorphism, *Rev. Geophys.*, *20*, 45–61, doi:10.1029/RG020i001p00045.

Contosta, A., et al. (2016), A longer vernal window: The role of winter coldness and snowpack in driving spring thresholds and lags, *Global Change Biol.*, doi:10.1111/gcb.13517.

Dang, C., R. E. Brandt, and S. G. Warren (2015), Parameterizations for narrowband and broadband albedo of pure snow and snow containing mineral dust and black carbon, *J. Geophys. Res. Atmos.*, *120*, 5446–5468, doi:10.1002/2014JD022646.

Delaney, I., S. Kaspari, and M. Jenkins (2015), Black carbon concentrations in snow at Tronsen Meadow in Central Washington from 2012 to 2013: Temporal and spatial variations and the role of local forest fire activity, *J. Geophys. Res. Atmos.*, *120*, 9160–9172, doi:10.1002/2015JD023762.

Déry, S. J., and R. D. Brown (2007), Recent Northern Hemisphere snow cover extent trends and implications for the snow-albedo feedback, *Geophys. Res. Lett.*, *34*, L22504, doi:10.1029/2007gl031474.

Diamond, H. J., et al. (2013), US Climate Reference Network after one decade of operations: Status and assessment, *Bull. Am. Meteorol. Soc.*, *94*(4), 485–498, doi:10.1175/BAMS-D-12-00170.1.

Doherty, S. J., C. Dang, D. A. Hegg, R. Zhang, and S. G. Warren (2014), Black carbon and other light-absorbing particles in snow of central North America, *J. Geophys. Res. Atmos.*, *119*, 12,807–12,831, doi:10.1002/2014JD022350.

Doherty, S. J., D. A. Hegg, J. E. Johnson, P. K. Quinn, J. P. Schwarz, C. Dang, and S. G. Warren (2016), Causes of variability in light absorption by particles in snow at sites in Idaho and Utah, *J. Geophys. Res. Atmos.*, *121*, 4751–4768, doi:10.1002/2015JD024375.

Douville, H., J. F. Royer, and J. F. Mahfouf (1995), A new snow parameterization for the Meteo-France climate model Part I: Validation in stand-along experiments, *Clim. Dyn.*, *1*(12), 21–35, doi:10.1007/BF00208760.

Draxler, R. R. (1999), HYSPLIT4 user's guide, NOAA Tech. Memo. ERL ARL-230, NOAA Air Resources Laboratory, Silver Spring, Md.

Draxler, R. R. and G. D. Hess (1997), Description of the HYSPLIT_4 modeling system, NOAA Tech. Memo. ERL ARL-224, 24 pp., NOAA Air Resources Laboratory, Silver Spring, Md.

Draxler, R. R., and G. D. Hess (1998), An overview of the HYSPLIT_4 modeling system of trajectories, dispersion, and deposition, *Aust. Meteor. Mag.*, *47*, 295–308.

Fierz, C., R. L. Armstrong, Y. Durand, P. Etchevers, E. Greene, D. M. McClung, K. Nishimura, P. K. Satyawali, and S. A. Sokratov (2009), *The international classification for seasonal snow on the ground*, UNESCO/IHP, Paris.

Flanner, M. G., and C. S. Zender (2006), Linking snowpack microphysics and albedo evolution, *J. Geophys. Res.*, *111*, D12208, doi:10.1029/2005jd006834.

Flanner, M. G., C. S. Zender, J. T. Randerson, and P. J. Rasch (2007), Present day climate forcing and response from black carbon in snow, *J. Geophys. Res.*, *112*, D11202, doi:10.1029/2006JD008003.

Fletcher, C. G., H. Zhao, P. J. Kushner, and R. Fernandes (2012), Using models and satellite observations to evaluate the strength of snow albedo feedback, *J. Geophys. Res.*, *117*, D11117, doi:10.1029/2012jd017724.

Gallet, J.-C., F. Domine, L. Arnaud, G. Picard, and J. Savarino (2011), Vertical profile of the specific surface area and density of the snow at Dome C and on a transect to Dumont D'Urville, Antarctica – albedo calculations and comparison to remote sensing products, *Cryosphere*, *5*, 631–649, doi:10.5194/tc-5-631-2011.

Grenfell, T. C., S. G. Warren, and P. C. Mullen (1994), Reflection of solar radiation by the Antarctic snow surface at ultraviolet, visible, and near-infrared wavelengths, *J. Geophys. Res.*, *99*, 18,669–18,684, doi:10.1029/94JD01484.

Groisman, P. Y., T. R. Karl, and R. W. Knight (1994), Observed impact of snow cover on the heat balance and the rise of continental spring temperatures, *Science*, *263*(5144), 198–200, doi:10.1126/science.263.5144.198.

Hadley, O. L., and T. W. Kirchstetter (2012), Black-carbon reduction of snow albedo, *Nat. Clim. Change*, *2*(6), 437–440, doi:10.1038/nclimate1433.

Hall, A., and X. Qu (2006), Using the current seasonal cycle to constrain snow albedo feedback in future climate change, *Geophys. Res. Lett.*, *33*, L03502, doi:10.1029/2005gl025127.

Hallett, J., and B. J. Mason (1958), The influence of temperature and supersaturation on the habit of ice crystals grown from the vapour, *Proc. R. Soc. A*, *247*, 440–453.

Hamilton, L. C., D. E. Rohall, B. C. Brown, G. F. Hayward, and B. D. Keim (2003), Warming winters and New Hampshire's lost ski areas: An integrated case study, *Int. J. Sociol. Social Policy*, *23*(10), 52–73, doi:10.1108/01443330310790309.

Hansen, J., and L. Nazarenko (2004), Soot climate forcing via snow and ice albedos, *Proc. Natl. Acad. Sci. U.S.A.*, *101*(2), 423–428, doi:10.1073/pnas.2237157100.

Huntington, T. G., G. A. Hodgkins, B. D. Keim, and R. W. Dudley (2004), Changes in the proportion of precipitation occurring as snow in New England (1949–2000), *J. Clim.*, *17*(13), 2626–2636, doi:10.1175/1520-0442(2004)017<2626:CITPOP>2.0.CO;2.

Kaspari, S., T. H. Painter, M. Gysel, S. M. Skiles, and M. Schwikowski (2014), Seasonal and elevational variations of black carbon and dust in snow and ice in the Solu-Khumbu, Nepal and estimated radiative forcings, *Atmos. Chem. Phys.*, *14*, 8089–8103, doi:10.5194/acp-14-8089-2014.

Kaspari, S., S. McKenzie Skiles, I. Delaney, D. Dixon, and T. H. Painter (2015), Accelerated glacier melt on Snow Dome, Mount Olympus, Washington, USA, due to deposition of black carbon and mineral dust from wildfire, *J. Geophys. Res. Atmos.*, *120*, 2793–2807, doi:10.1002/2014JD022676.

Knowles, N., M. D. Dettinger, and D. R. Cayan (2006), Trends in snowfall versus rainfall in the western United States, *J. Clim.*, *19*(18), 4545–4559, doi:10.1175/JCLI3850.1.

Kokhanovsky, A. A., and E. P. Zege (2004), Scattering optics of snow, *Appl. Opt.*, *43*(7), 1589–1602, doi:10.1364/AO.43.001589.

Lazarcik, J., J. E. Dibb, A. C. Adolph, J. M. Amante, C. P. Wake, E. Scheuer, M. M. Mineau, and M. R. Albert, (2016), Major fraction of black carbon is flushed from the melting New Hampshire snowpack nearly as quickly as soluble impurities, *J. Geophys. Res. Atmos.*, doi:10.1002/2016JD025351.

Lhermitte, S., J. Abermann, and C. Kinnard (2014), Albedo over rough snow and ice surfaces, *Cryosphere*, *8*(3), 1069–1086, doi:10.5194/tc-8-1069-2014.

Libbrecht, K. G. (2005), The physics of snow crystals, *Rep. Prog. Phys.*, *68*, 855–895, doi:10.1088/0034-4885/68/4/R03.

Meinander, O., et al. (2013), Spectral albedo of seasonal snow during intensive melt period at Sodankylä, beyond the Arctic Circle, *Atmos. Chem. Phys.*, *13*(7), 3793–3810, doi:10.5194/acp-13-3793-2013.

Nolin, A. W., and J. Dozier (2000), A hyperspectral method for remotely sensing the grain size of snow, *Remote Sens. Environ.*, *74*(2), 207–216, doi:10.1016/s0034-4257(00)00111-5.

Oaida, C. M., Y. Xue, M. G. Flanner, S. M. Skiles, F. De Sales, and T. H. Painter (2015), Improving snow albedo processes in WRF/SSiB regional climate model to assess impact of dust and black carbon in snow on surface energy balance and hydrology over western U.S, *J. Geophys. Res. Atmos.*, *120*, 3228–3248, doi:10.1002/2014JD022444.

Oleson, K. W., et al. (2010), Technical description of version 4.0 of the Community Land Model (CLM).

Painter, T. H., J. Dozier, D. A. Roberts, R. E. Davis, and R. O. Green (2003), Retrieval of subpixel snow-covered area and grain size from imaging spectrometer data, *Remote Sens. Environ.*, *85*, 64–77, doi:10.1016/S0034-4257(02)00187-6.

Painter, T. H., N. P. Molotch, M. Cassidy, M. Flanner, and K. Steffen (2007a), Contact spectroscopy for determination of stratigraphy of snow optical grain size, *J. Glaciol.*, *53*(180), 121–127, doi:10.3189/172756507781833947.

Painter, T. H., A. P. Barrett, C. C. Landry, J. C. Neff, M. P. Cassidy, C. R. Lawrence, K. E. McBride, and G. L. Farmer (2007b), Impact of disturbed desert soils on duration of mountain snow cover, *Geophys. Res. Lett.*, *34*, L12502, doi:10.1029/2007GL030284.

Painter, T. H., J. S. Deems, J. Belnap, A. F. Hamlet, C. C. Landry, and B. Udall (2010), Response of Colorado River runoff to dust radiative forcing in snow, *Proc. Natl. Acad. Sci. U.S.A.*, *107*(40), 17,125–17,130, doi:10.1073/pnas.0913139107.

Painter, T. H., S. M. Skiles, J. S. Deems, A. C. Bryant, and C. C. Landry (2012), Dust radiative forcing in snow of the Upper Colorado River Basin: 1. A 6 year record of energy balance, radiation, and dust concentrations, *Water Resour. Res.*, *48*, W07521, doi:10.1029/2012WR011985.

Pedersen, C. A., J. C. Gallet, J. Ström, S. Gerland, S. R. Hudson, S. Forsström, E. Isaksson, and T. K. Berntsen (2015), In situ observations of black carbon in snow and the corresponding spectral surface albedo reduction, *J. Geophys. Res. Atmos.*, *120*, 1476–1489, doi:10.1002/2014jd022407.

Peng, S., S. Piao, P. Ciais, P. Friedlingstein, L. Zhou and T. Wang (2013), Change in snow phenology and its potential feedback to temperature in the Northern Hemisphere over the last three decades, *Environ. Res. Lett.*, *8*(1), 014008, doi:10.1088/1748-9326/8/1/014008.

Perovich, D. K. (2007), Light reflection and transmission by a temperate snow cover, *J. Glaciol.*, *53*(181), 201–210, doi:10.3189/172756507782202919.

Perovich, D. K., T. C. Grenfell, B. Light, and P. V. Hobbs (2002), Seasonal evolution of the albedo of multiyear Arctic sea ice, *J. Geophys. Res.*, *107*(C10), 8044, doi:10.1029/2000JC000438.

Picard, G., Q. Libois, L. Arnaud, G. Verin, and M. Dumont (2016), Development and calibration of an automatic spectral albedometer to estimate near-surface snow SSA time series, *Cryosphere*, *10*, 1297–1316, doi:10.5194/tc-10-1297-2016.

Polashenski, C. M., J. E. Dibb, M. G. Flanner, J. Y. Chen, Z. R. Courville, A. M. Lai, J. J. Schauer, M. M. Shafer, and M. Bergin (2015), Neither dust nor black carbon causing apparent albedo decline in Greenland᾿s dry snow zone: Implications for MODIS C5 surface reflectance, *Geophys. Res. Lett.*, *42*, 9319–9327, doi:10.1002/2015GL065912.

Putman, A. (2013), Tracking the moisture sources of storms at Barrow, Alaska: Seasonal variations and isotopic characteristics, MS Thesis. Dartmouth College, 102; 1553179, ISBN:9781303773570.

Qian, Y., W. I. Gustafson, L. R. Leung, and S. J. Ghan (2009), Effects of soot-induced snow albedo change on snowpack and hydrological cycle in western United States based on Weather Research and Forecasting chemistry and regional climate simulations, *J. Geophys. Res.*, *114*, D03108, doi:10.1029/2008jd011039.

Qian, Y., T. J. Yasunari, S. J. Doherty, M. G. Flanner, W. K. M. Lau, J. Ming, H. Wang, M. Wang, S. G. Warren, and R. Zhang (2015), Light-absorbing particles in snow and ice: Measurement and modeling of climatic and hydrological impact, *Adv. Atmos. Sci.*, *32*(1), 64–91, doi:10.1007/s00376-014-0010-0.

Qu, X., and A. Hall (2007), What controls the strength of snow-albedo feedback?, *J. Clim.*, *20*(15), 3971–3981, doi:10.1175/jcli4186.1.

Qu, X., and A. Hall (2014), On the persistent spread in snow-albedo feedback, *Clim. Dyn.*, *42*(1–2), 69–81, doi:10.1007/s00382-013-1774-0.

Ramanathan, V., and G. Carmichael (2008), Global and regional climate changes due to black carbon, *Nat. Geosci.*, *1*(4), 221–227, doi:10.1038/ngeo156.

Sall, J. (1990), Leverage plots for general linear hypotheses, *Am. Stat.*, *44*(4), 308–315, doi:10.2307/2684358.

Singh, S. K., A. V. Kulkarni, and B. S. Chaudhary (2010), Hyperspectral analysis of snow reflectance to understand the effects of contamination and grain size, *Ann. Glaciol.*, *51*, 83–88, doi:10.3189/172756410791386535.

Skiles, S. M. (2014), *Dust and Black Carbon Radiative Forcing Controls on Snowmelt in the Colorado River Basin*, UCLA, Los Angeles, Calif.

Skiles, S. M., T. H. Painter, J. Deems, and C. C. Landry (2012), Dust radiative forcing in snow of the Upper Colorado River Basin: Part II. Interannual variability in radiative forcing and snowmelt rates, *Water Resources Research*, *48*, W07522, doi:10.1029/2012WR011986.

Skiles, S. M., T. H. Painter, J. Belnap, L. Holland, R. L. Reynolds, H. L. Goldstein, and J. Lin (2015), Regional variability in dust-on-snow processes and impacts in the Upper Colorado River Basin, *Hydrol. Process.*, *29*, 5397–5413, doi:10.1002/hyp.10569.

Slater, A. G., A. J. Pitman, and C. E. Desborough (1998), The validation of a snow parameterization designed for use in general circulation models, *Int. J. Climatol.*, *18*(6), 595–617, doi:10.1002/(SICI)1097-0088(199805)18:6<595::AID-JOC275>3.0.CO;2-O.

Steffensen, J. P. (1997), The size distribution of microparticles from selected segments of the Greenland Ice Core Project ice core representing different climatic periods, *J. Geophys. Res.*, *102*, 26,755–26,763, doi:10.1029/97JC01490.

Sterle, K. M., J. R. McConnell, J. Dozier, R. Edwards, and M. G. Flanner (2013), Retention and radiative forcing of black carbon in eastern Sierra Nevada snow, *Cryosphere*, *7*, 365–374, doi:10.5194/tc-7-365-2013.

Intergovernmental Panel on Climate Change (IPCC) (2013), *Climate Change 2013: The Physical Science Basis. Contribution of Working Group I to the Fifth Assessment Report of the Intergovernmental Panel on Climate Change*, edited by T. F. Stocker et al., 1535 pp., Cambridge Univ. Press, Cambridge, U. K., and New York, doi:10.1017/CBO9781107415324.

Trenberth, K. E. (2011), Changes in precipitation with climate change, *Clim. Res.*, *47*(1), 123–138, doi:10.3354/cr00953.

Tukey, J. W. (1949), Comparing individual means in the analysis of variance, *Biometrics*, *5*(2), 99–114, doi:10.2307/3001913.

Verseghy, D. L. (1991), Class—A Canadian land surface scheme for GCMS, I. Soil model, *Int. J. Climatol.*, *11*, 111–133, doi:10.1002/joc.3370110202.

Warren, S. G., and W. J. Wiscombe (1980), A model for the spectral albedo of snow. II: Snow containing atmospheric aerosols, *J. Atmos. Sci.*, *37*(12), 2734–2745, doi:10.1175/1520-0469(1980)037%3C2734:amftsa%3E2.0.co;2.

Weiss, A. and J. M. Norman (1985), Partitioning solar radiation into direct and diffuse, visible and near-infrared components, *Agric. For. Meteorol.*, *34*, 205–213, doi:10.1016/0168-1923(85)90020-6.

White, M. A., et al. (2009), Intercomparison, interpretation, and assessment of spring phenology in North America estimated from remote sensing for 1982–2006, *Global Change Biol.*, *15*(10), 2335–2359, doi:10.1111/j.1365-2486.2009.01910.x.

Wiscombe, W. J., and S. G. Warren (1980), A model for the spectral albedo of snow. I: Pure snow, *J. Atmos. Sci.*, *37*(12), 2712–2733, doi:10.1175/1520-0469(1980)037<2712:amftsa>2.0.co;2.

Wright, P., et al. (2014), Comparing MODIS daily snow albedo to spectral albedo field measurements in central Greenland, *Remote Sens. Environ.*, *140*, 118–129, doi:10.1016/j.rse.2013.08.044.

Yasunari, T. J., R. D. Koster, W. K. M. Lau, and K.-M. Kim (2015), Impact of snow darkening via dust, black carbon, and organic carbon on boreal spring climate in the Earth system, *J. Geophys. Res. Atmos.*, *120*, 5485–5503, doi:10.1002/2014JD022977.